REPORT DOCUMENTATION PAGE

Form Approved
OMB No. 0704-0188

1. AGENCY USE ONLY (Leave Blank)	2. REPORT DATE	3. REPORT TYPE AND DATES COVERED
	1 June 2001	Final (03/15/99 – 03/31/00)

4. TITLE AND SUBTITLE
Effect of shallow water internal waves on ocean acoustic striation patterns

5. FUNDING NUMBERS
N00014-99-1-0494

6. AUTHOR(S)
Daniel Rouseff

7. PERFORMING ORGANIZATION NAME(S) AND ADDRESS(ES)
Applied Physics Laboratory
University of Washington
1013 NE 40th St.
Seattle, WA 98105-6698

8. PERFORMING ORGANIZATION REPORT NUMBER

9. SPONSORING/MONITORING AGENCY NAME(S) AND ADDRESS(ES)
Office of Naval Research
Program Officer Jeffrey Simmen, Code 321OA
800 N. Quincy St.
Arlington, VA 22217-5660

10. SPONSORING/MONITORING AGENCY REPORT NUMBER

11. SUPPLEMENTARY NOTES

The report has been submitted to the journal *Waves in Random Media*. Publication is expected later in 2001.

12a. DISTRIBUTION/AVAILABILITY STATEMENT

Approved for public release

12b. DISTRIBUTION CODE

13. ABSTRACT (Maximum 200 words)

Contour plots of underwater acoustic intensity, mapped in range and frequency, often exhibit striations. It has been claimed that a scalar parameter "beta," defined in terms of the slope of the striations, is invariant to the details of the acoustic waveguide. In shallow water, the canonical value for beta is one. In the present paper, the waveguide invariant is modeled as a distribution rather than a scalar. The effects of shallow water internal waves on the distribution are studied by numerical simulation. Realizations of time-evolving shallow water internal wave fields are synthesized and acoustic propagation simulated using the parabolic equation method. The waveguide invariant distribution is tracked as the internal wave field evolves in time. Both random background internal waves and more event-like solitary internal waves are considered.

14. SUBJECT TERMS
underwater acoustic intensity, acoustic waveguide, internal waves, acoustic signal processing

15. NUMBER OF PAGES
19

16. PRICE CODE

17. SECURITY CLASSIFICATION OF REPORT	18. SECURITY CLASSIFICATION OF THIS PAGE	19. SECURITY CLASSIFICATION OF ABSTRACT	20. LIMITATION OF ABSTRACT
Unclassified	Unclassified	Unclassified	UL

Effect of shallow water internal waves on ocean acoustic striation patterns

Daniel Rouseff
Applied Physics Laboratory
College of Ocean and Fishery Sciences
1013 NE 40th Street, Seattle, WA 98105

Abstract. Contour plots of underwater acoustic intensity, mapped in range and frequency, often exhibit striations. It has been claimed that a scalar parameter "beta," defined in terms of the slope of the striations, is invariant to the details of the acoustic waveguide. In shallow water, the canonical value is $\beta = 1$. In the present paper, the waveguide invariant is modeled as a distribution rather than a scalar. The effects of shallow water internal waves on the distribution are studied by numerical simulation. Realizations of time-evolving shallow water internal wave fields are synthesized and acoustic propagation simulated using the parabolic equation method. The waveguide invariant distribution is tracked as the internal wave field evolves in time. Both random background internal waves and more event-like solitary internal waves are considered.

Note: A version of this report was submitted to the journal *Waves in Random Media.*

1. Introduction

In the second edition of *Fundamentals of Ocean Acoustics,* Brekhovskikh and Lysanov introduced the concept of intensity invariance to a larger audience [1]. They showed the acoustic intensity plotted versus range and frequency would exhibit striations, parallel contours of high intensity. They defined a parameter "beta" as a simple function of range, frequency and the slope of the striations, and claimed that this parameter was invariant. For a deep-water scenario with a sound speed duct, they found $\beta = -3$. In shallow water, they assumed an isovelocity water column and found $\beta = +1$.

The concept of a waveguide invariant has enormous appeal. The waveguide might support several mutually interfering acoustic modes. The interference between the modes will change with acoustic frequency. If the invariant concept is valid, the complicated details of an interference pattern can be distilled into a single scalar parameter. This would be particularly useful in shallow water where the sound may have multiple interactions with both the sea surface and the seabed. From a modest knowledge of the medium, beta could be estimated and compared to measurements. Beta constitutes a robust observable; while the details of the intensity striation pattern may change in time, the waveguide invariant should remain constant if it is truly invariant.

Beginning with the article by Chuprov [2], a number of Russian papers examine different aspects of the waveguide invariant problem. The more theoretical of these studies relied on analytical techniques. Perturbation theory, adiabatic modes, the WKB approximation and other simplifications were necessary to get closed form solutions [3-6]. More recently, the concept has received attention in the Western literature [7]. It was used to move the focal range in a phase conjugation experiment [8]. The theory was extended to environments varying in azimuth and used in the analysis of single receiver spectrograms [9].

Shallow water is often characterized by strong stratification in temperature and density. Disturbances to the pycnocline induced by tidal forcing cause internal waves to be generated. From the standpoint of acoustics, internal waves cause fluctuations in the speed of sound and so distort a propagating acoustic field. Petnikov and colleagues [10-12] have shown that shallow water variability, including internal waves, can cause the interference pattern of the acoustic field to shift in frequency. The goal of the present work is to determine if the "waveguide invariant" is truly "invariant" to effects of internal waves, or if the frequency shifts they introduce are sufficient to destroy the concept.

In Section 2, intensity invariance is examined by numerical simulation for range-independent environments. When there is a sound speed profile, the slope of the intensity striations is shown to depend on the depth of the receiver. These simulations serve primarily as the baseline to which other more complicated scenarios will be compared. A new method for quantifying the "beta content" of intensity images is outlined in Section 3. Rather than treat the waveguide invariant as a scalar, it is modeled as a distribution. The shape of the distribution will depend on the propagation environment and the measurement geometry; the distribution can be sharply peaked around a single value or more diffuse. Random background internal waves are considered in Section 4. Realizations of time-evolving shallow water internal waves are synthesized and acoustic propagation through the range-dependent environment is simulated using the parabolic equation method. The waveguide invariant distribution is estimated from images of intensity and tracked as the internal wave field evolves. Depending on several factors, the internal waves can have significantly different effects on the distribution: it can be left practically unchanged, made more sharp around a single value, or become more diffuse. The distribution can even become bimodal making it appear as if there were two sources. These effects can be explained by mode

coupling. A simple model for solitary internal waves is used in Section 5. Solitary wave motion is shown to cause rapid changes in the waveguide invariant distribution.

2. Range-independent Scenarios

The concept of a waveguide invariant is most easily illustrated by an example. Consider an isovelocity water column, 70 m deep, with sound speed 1480 m/s. The bottom is also range-independent with sound speed 1580 m/s, density 1.85 g/cm^3, and attenuation 0.04 dB/λ. Place an acoustic source at depth 50 m, and consider the downrange intensity calculated at the same depth. Figure 1 shows the transmission loss over a window from 9 to 10 km downrange, and from 400 to 420 Hz. The image was sampled every 4 m in range and every 0.25 Hz in frequency. The calculation assumes the source has a flat response over this frequency band. The scale spans a 16 dB dynamic range. The image shows clear striations.

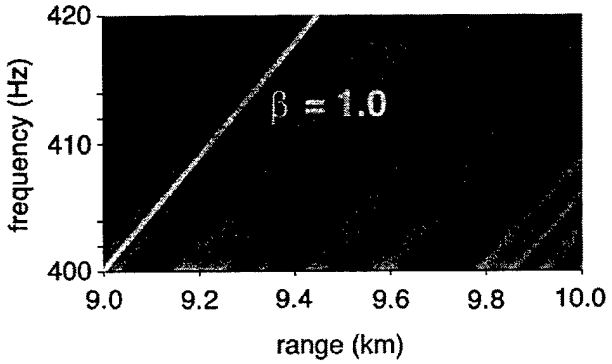

Figure 1. Transmission loss in range-frequency plane. Range is distance from source at constant depth 50 m. Isovelocity water column 70 m deep. Remaining simulation parameters described in the text. Color scale spans 16 dB dynamic range. Line superimposed on image corresponds to invariant parameter beta equal one.

Superimposed on the image is a line along the crest of one of the nearly parallel striations. Define the slope of this line as $d\omega/dr$. Let $I(r,\omega)$ be the intensity as a function of range and frequency. Then along the crest

$$(d\omega\,\hat{\omega} + dr\,\hat{r})\cdot\nabla I = 0, \tag{1}$$

which implies

$$\frac{d\omega}{dr} = -\frac{\partial I/\partial r}{\partial I/\partial \omega}. \tag{2}$$

Brekhovshikh and Lysanov define the parameter β as

$$\beta = \frac{r}{\omega}\frac{d\omega}{dr} \tag{3}$$

and claim it to be invariant. That is, if one were to increase the frequency, for example, the slope of the striations would increase so as to leave β unchanged. If one were to increase the range, the slope would be more shallow. Consequently, if it is truly invariant, this single scalar parameter captures many of the essential features of the propagating acoustic energy.

The line in Fig. 1 corresponds to β =1, the canonical value for shallow water. To understand its origins, expand the acoustic intensity in its normal modes [1,2]. Assuming a range-independent environment with source and receiver depths z_s and z, respectively

$$I = \left| \sum_m (\xi_m r)^{-1/2} \Psi_m(z_s) \Psi_m(z) e^{i\xi_m r} \right|^2 \equiv \sum_{m,n} B_{m,n} \cos[(\xi_m - \xi_n) r], \tag{4}$$

where Ψ_m is an eigenfunction (mode) and ξ_m the corresponding eigenvalue (horizontal wavenumber). These terms are subsumed in $B_{m,n}$, and certain unimportant scaling terms have been suppressed. Taking the derivative with respect to range yields

$$\begin{aligned} \partial I/\partial r &\approx -\sum_{m,n} B_{m,n} (\xi_m - \xi_n) \sin[(\xi_m - \xi_n) r] \\ &= -\omega \sum_{m,n} B_{m,n} \left(\frac{1}{v_m} - \frac{1}{v_n} \right) \sin[(\xi_m - \xi_n) r] \end{aligned} \tag{5}$$

where $v_m = \omega/\xi_m$ is the phase velocity of the corresponding mode. The expression is approximate because the weak range-dependence of $B_{m,n}$ has been neglected. Similarly, taking the derivative with respect to frequency

$$\partial I/\partial \omega \approx -r \sum_{m,n} B_{m,n} \left(\frac{1}{u_m} - \frac{1}{u_n} \right) \sin[(\xi_m - \xi_n) r], \tag{6}$$

where $u_m = \left(\partial \xi_m / \partial \omega\right)^{-1}$ is the group velocity.

Equations (5) and (6) can be substituted into Eq. (2), and the result substituted into (3). Note that the explicit r and ω in (3) are both cancelled by terms in the intensity derivatives. Still, the result is a cumbersome ratio of summations, with phase velocity terms in the numerator and group velocity terms in the denominator. The expression simplifies, however, when one realizes that there is typically a functional dependence between the group and phase velocities. For example, consider an isovelocity waveguide bounded from above by the sea surface and from below by a perfectly reflecting bottom. One can show [1] that the product of the two velocities is a constant, independent of mode number: $u_m v_m = C^2$. When this is substituted into (3), it follows that first order changes in phase and group velocities contribute only higher order changes in β; literally, the expression is invariant and β =1 is the correct numerical value. The situation in Fig. 1 differs only slightly in that the bottom is penetrable and has some associated loss.

More complicated scenarios would involve a sound speed profile in the water column. In this case, Brekhovskikh and Lysanov approximate the relationship between the phase and group velocities by a power series and retain terms only through first order. Within these approximations, β remains invariant, but its numerical value could change.

As an example, consider the sound speed profile shown in Fig. 2. A mixed layer extends down to about 12 m followed by a fairly steep thermocline. The sound speed gradient gradually lessens, and below about 45 m the water is nearly isovelocity down to the bottom at 70 m. Also

shown are the first four acoustic modes. The first mode has an upper turning point in the thermocline, well below the sea surface. The next few modes also turn in the water column, reaching the sea surface only in their asymptotic region, if at all. Only by mode 7 (not shown) are the modes clearly bound from above by the sea surface. This differs from the isovelocity case where all the modes reach the sea surface.

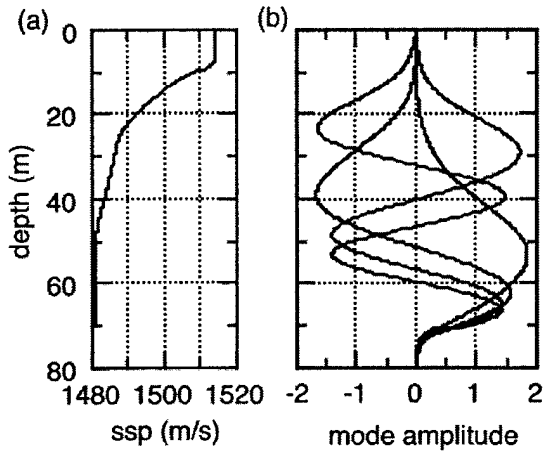

Figure 2. Depth dependent environment. (a) Sound speed profile in water column, and (b) associated first four acoustic modes. In Section 3, the profile is perturbed by internal waves introducing range dependence in the environment.

The sound speed profile in Fig. 2 was used in an acoustic simulation. The remaining simulation parameters were the same as in Fig. 1, with the source still at depth 50 m. Figure 3 shows the simulated intensity pattern at two depths: 10 and 50 m. Although not as pristine as Fig. 1, both patterns show striations. Consider Fig. 3(a) where the receiver is above the thermocline. The low order modes turn below the shallow receiver and so the propagation is dominated by the higher order modes. These higher order modes interact with the sea surface and as a result $\beta = 1$ remains a reasonable value. The situation changes for the deep receiver, Fig. 3(b). The intensity is dominated by the less attenuated, lower order modes. The striation pattern is steeper, and while the concept of an invariant remains plausible a larger numerical value is in order. The result is consistent with a recent field experiment where both source and receivers were below the thermocline and $\beta = 1.4$ was observed [8].

Figures 1 and 3 show lines corresponding to different values of beta. To draw these lines, the relationship in (3) was approximated by setting the range to 9 km, the frequency to 400 Hz, and replacing the derivative by a finite difference. A more systematic way of analyzing intensity images is derived in the following section.

3. Modeling the waveguide invariant as a distribution

Brekhovskikh and Lysanov [1] cautioned that the definition of β in (1) applies only "for a group of modes." As the range and frequency change, "the sound field will be determined by another group of modes...result[ing] in a change of β." Internal waves cause the acoustic modes to couple, potentially causing the field to be determined by a different group of modes and thereby changing beta. For example, the water borne modes in Fig. 2(b) will have a different value of beta than the higher order modes that interact with the sea surface. Internal waves will cause the distribution of energy in the different acoustic modes to change in time and space and thereby change the distribution of values for beta.

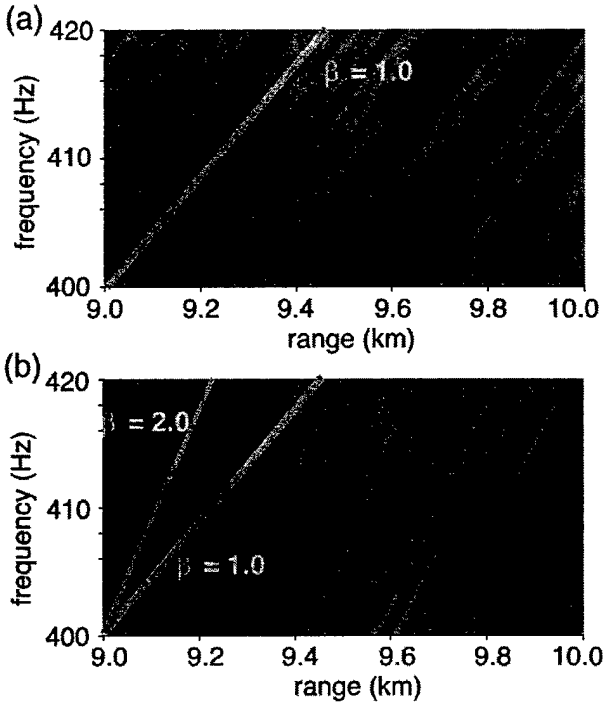

Figure 3. Transmission loss in range-frequency plane. Water column described by sound speed profile in Fig. 2. (a) Receiver depth 10 m. (b) Receiver depth 50 m. Same color scale as in Fig. 1.

In his original paper [2], Chuprov suggested that "in more-complex situations, spectral analysis of experimental values of intensity as a function of two arguments $I(\omega,r)$ should be used." In this section, a new spectral method for analyzing intensity images is developed. As an output of this processing, beta is treated as a distribution rather than a simple scalar parameter. Effectively, one calculates the "beta content" of the measured intensity. In subsequent sections, this processing method is used to quantify the effect of internal waves.

Let the intensity pattern $I(r,\omega)$ be measured over the finite window $r_{\min} < r < r_{\max}$ and $\omega_{\min} < \omega < \omega_{\max}$. The data window is assumed small compared to the dimensions of the problem:

$$\begin{aligned} r_{\text{mid}} &\equiv (r_{\max} + r_{\min})/2 >> (r_{\max} - r_{\min}), \\ \omega_{\text{mid}} &\equiv (\omega_{\max} + \omega_{\min})/2 >> (\omega_{\max} - \omega_{\min}). \end{aligned} \tag{7}$$

Because the pattern is expected to exhibit striations, model $I(r,\omega)$over the data window as:

$$I(r,\omega) \approx I_1\left(r - (d\omega/dr)^{-1}\omega\right). \tag{8}$$

where recall $d\omega/dr$ is the slope of the striations. The function $I_1(r)$ is determined by the interference between the propagating modes at a single frequency; see (4). The details of this one-dimensional function are less important than the fact that it can be used to approximate the striated two-dimensional function $I(r,\omega)$. Evaluate (3) at r_{mid} and ω_{mid}, and substitute into (8):

$$I(r,\omega) \approx I_1\left(r - \mu\omega\right) \tag{9}$$

where

$$\mu = (r_{\text{mid}}/\omega_{\text{mid}})\beta^{-1}. \tag{10}$$

Estimating a numerical value for β from a given image is perhaps most easily done in the Fourier domain. Define the transform

$$\tilde{I}(\kappa,\tau) = \int_{-\infty}^{\infty}\int_{-\infty}^{\infty} I(r,\omega)e^{i(\kappa r+\omega\tau)}drd\omega. \tag{11}$$

Strictly speaking, the model should be applied only over the finite data window. If it is artificially applied over the entire region of integration in (11), a particularly simple formula results:

$$\tilde{I}(\kappa,\tau) \approx \tilde{I}_1(\kappa)\delta(\tau+\mu\kappa). \tag{12}$$

The delta function in (12) means that the two-dimensional transform is non zero only along the line $\tau = -\mu\kappa$ in Fourier space. The slope of the line, $-\mu$, determines β via (10). In practice, (12) would be convolved with the finite sized data window and the line would be smeared. The point remains, however, that from the Fourier transform of the image one can determine β.

The argument can be generalized to quantify the "beta content" of arbitrary intensity images. Let $< I >$ be the mean intensity averaged over the data window. Define $I_0 = I - < I >$. Then by Parseval's theorem, the energy E in the two domains is equivalent:

$$E \equiv \int_{-\infty}^{\infty}\int_{-\infty}^{\infty} |I_0(r,\omega)|^2 drd\omega = (2\pi)^{-2}\int_{-\infty}^{\infty}\int_{-\infty}^{\infty} \left|\tilde{I}_0(\kappa,\tau)\right|^2 d\kappa d\tau. \tag{13}$$

Converting the latter to the polar coordinates $\kappa = K\cos\phi$ and $\tau = K\sin\phi$ yields

$$E = \int_{-\pi/2}^{\pi/2} E_\beta d\phi \tag{14}$$

where

$$E_\beta = (2\pi)^{-2}\int_{-B}^{B} \left|\tilde{I}_0(K\cos\phi, K\sin\phi)\right|^2 |K| dK. \tag{15}$$

The integral has been truncated at some maximum spatial frequency of interest B. The ramp filter $|K|$ in (15) arises from the change of variables. Note that $\tilde{I}_0(K\cos\phi, K\sin\phi)$ is the transform evaluated along a line in Fourier space passing through the origin at angle ϕ. Using (10), this angle can be related to β:

$$\beta = -r_{mid}/(\omega_{mid}\tan\phi). \tag{16}$$

Equation (15) can be evaluated over a range of angles thereby defining E_β as a distribution. Effectively, one calculates the "beta content" of an image. Figure 4 shows the function $\pi E_\beta/E$ plotted versus β for the cases considered in Figs. 1 and 3. This normalization means the distribution would equal one if the energy were uniformly distributed in angle. As expected, the distributions for the two cases where there is significant interaction with the sea surface have their maxima near $\beta = 1$. For the case with both source and receiver below the thermocline, the

distribution is more spread and the maximum shifted to near $\beta = 1.5$. Note the small secondary maximum for this case near $\beta = 1$. This peak is from the interaction between the higher order, surface interacting modes.

The proposed method of analysis has some useful features. Note that the $(I - < I >)^2$ used in the formulation literally defines the scintillation, a physically meaningful quantity [13]. Plots such as Fig. 4 identify the most likely value for β but also show the spread. Note also that $\tilde{I}_0(K\cos\phi, K\sin\phi)$ used in the present development can be related to the Radon transform by the well-known Projection-Slice theorem of tomography [14]; recently, Thode [15] analyzed intensity images using the Radon transform. For real or synthetic data measured over a finite data window, the continuous Fourier transform in (15) can be approximated using the FFT. Interpolation and numerical quadrature then approximate the integral in (15).

For range-independent environments, Rouseff and Spindel were able to derive a simple formula relating the beta distribution to the modal expansion of the field and the measurement geometry [16]. The source and/or receiver depths were varied, and the effects of bottom loss quantified. Such a simple decomposition, however, is not possible when there is range-dependence in the environment. In the following sections, the effects of range-dependent shallow water internal waves are studied.

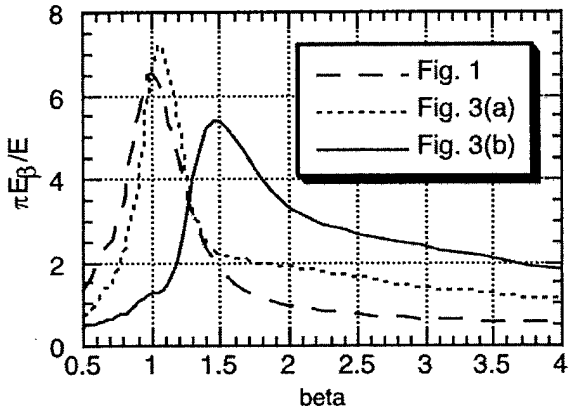

Figure 4. "Beta content" of images. Using discrete version of Eq. (15), calculated and plotted versus beta for images shown in Figs. 1, 3(a) and 3(b). For the two cases with significant energy in surface interacting acoustic modes, the maximum is at the canonical value beta equal one. A higher value is appropriate when both source and receiver are below the thermocline.

4. Effect of Background Internal Waves

In deep water, internal waves propagate in many different directions. Since the waves are randomly phased, it is appropriate to model them as a random process governed by a spectrum. These waves induce fluctuations in the sound speed and so affect acoustic energy propagating through them. The success of the Garrett-Munk (GM) approach [17] in deep water has lead to speculation that a similar model might be useful for shallow water situations. While this remains a research topic [18-20], it appears that diffuse background internal waves in shallow water can be represented by a GM-like model. In this section, a spectral model developed from a recent shallow water field experiment is used to specify an ocean internal wave simulator. Acoustic propagation through the resulting sound field is accomplished using a parabolic equation method. The beta distribution is estimated from images of acoustic intensity and tracked as the internal wave field evolves.

Two parameters of the GM internal wave model are the modal bandwidth, given by j_*, and the strength, given by the product bE_{GM}; see Henyey et al. [18] for details. The parameters for the shallow water situation in this work are determined by moored temperature and current

measurements obtained by a group at Oregon State University [21] concurrent with the 1996 Coastal Mixing and Optics Experiment [22]. As has been observed in several experiments [23], the shallow water measurements indicate an internal wave field dominated by low-order modes. A value of $j_* = 0$ is supported by the observed depth dependence of current variance. The small value for j_* means certain approximations that are standard for deep water, particularly those derived from the WKB method, are not adequate. Consequently, the full internal wave mode functions must be calculated using numerical techniques. Values of bE_{GM} from the data vary from 0.35 to 0.5 m, the larger value being used here. Note that the model was developed for a relatively quiescent period when solitary waves were absent.

The sound speed fluctuations caused by the internal waves are assumed to arise solely from the displacements, and current fluctuations are neglected. The spectral model was used as input to an ocean simulator [24]. The simulator is a numerical solution to the linear internal wave equations and produces fully three-dimensional realizations. Although the acoustic problem requires only slices in range and depth, the complexity of a three-dimensional field is needed to evolve the internal waves in time properly. In the present application, a computational domain 70 m deep by 21 km in range by 5.25 km in the transverse direction was used. Range-depth slices were obtained from each three dimensional realization.

The resulting internal wave displacements $\zeta(r,z)$ are converted to sound speed perturbations $\delta C(r,z)$. These are then added to the mean background profile $\overline{C}(z)$. The sound speed profile shown in Fig. 2, obtained from the moored measurements [21], represents the mean environment. There are some subtle issues in converting from wave displacement to sound speed. In deep water, $\delta C(r,z)$ is usually obtained from $\zeta(r,z)$ by a first order Taylor expansion [25]. In shallow water, the vertical sound speed gradients change rapidly rendering the expansion questionable. Since the displacements are known exactly from the simulation, the more accurate conversion is used:

$$\delta C(r,z) = \overline{C}_p(z - \zeta(r,z)) - \overline{C}_p(z), \tag{17}$$

where $\overline{C}_p(z)$ is the mean potential sound speed.

Sound propagation through the resulting environment was calculated using a parabolic equation routine. The simulations were repeated at numerous acoustic frequencies. The entire suite of simulations was repeated at each time step as the internal wave field was allowed to evolve. At each time step, the beta distribution was calculated by implementing a discrete version of the processor (15). In the following subsections, different parameters of the simulation are varied.

4.a. Receiver depth

The depth-dependent scenario of Section 2 was modified by the inclusion of range-dependent internal waves. The acoustic source was fixed at depth 50 m. The data window for the intensity images remained from 9 to 10 km in range, 400 to 420 Hz in frequency. The intensity was sampled every 4 m in range, every 0.25 Hz in frequency.

First consider a receiver below the thermocline at 50 m depth. Figure 5 shows the beta distribution evolving over three hours. The time step between curves is 400 seconds. So that they could be compared, the E_β at each time step was normalized by the total energy in the range-independent case, Fig. 3(b).

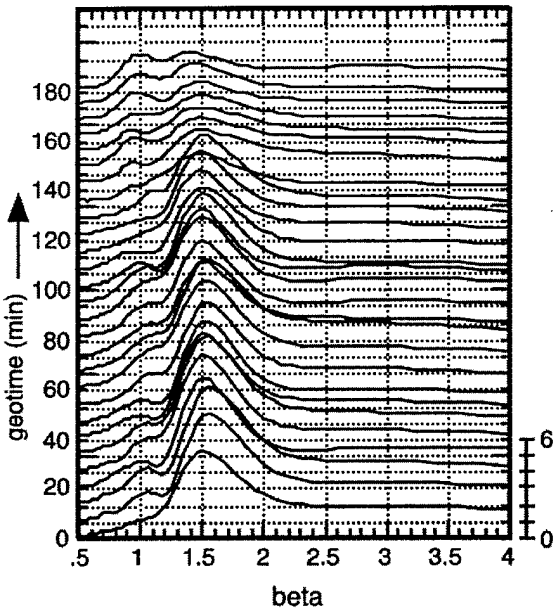

Figure 5. Effect of evolving background internal waves on intensity invariant. Time step between curves is 400 seconds. Both source and receiver below the thermocline at depth 50 m. Remaining simulation parameters described in text.

Several observations can be made. The maximum value of E_β changes in time. In part, this is a matter of serendipity. As suggested by Petnikov and Kuz'kin [10], the internal waves shift the locations of the intensity striations in range and frequency. At certain times, the bands of high intensity are centrally located in the 1 km-by-20 Hz data window and the maximum value of E_β increases. At other times, the bands are shifted out of the main data window and E_β decreases. Note that while the details of the distribution change, there is a persistent maximum at around $\beta = 1.5$, the value for the range-independent case. Consequently, in a practical sense, the "invariant parameter" is indeed invariant to the fluctuations induced by internal waves for this case.

Interestingly, in addition to the persistent maximum near $\beta = 1.5$, there is an intermittent local maximum near $\beta = 1$. At 180 minutes, for example, the value of E_β at $\beta = 1$ is comparable to that observed at $\beta = 1.5$. The distribution has become bimodal with two distinct peaks. It is as if the observed intensity pattern was produced by two different acoustic sources. This is an artifact of acoustic mode coupling. The internal waves have driven energy into the higher order, surface-interacting modes. These modes, as shown in the previous section, give rise to the maximum near $\beta = 1$.

Figure 6 shows the evolving beta content for a receiver above the thermocline at 10 m depth. The same realization of the internal wave field is used, and the remaining simulation parameters are unchanged. At each time step, E_β is normalized by the total energy in the range-independent case, Fig. 3(a). The maximum at $\beta = 1$ is strong and persistent. Note that there are instances where the maximum exceeds 7.2, the value for the range-independent case (see Fig. 4). The internal waves have actually enhanced the $\beta = 1$ content of the images. Comparing to Fig. 5, it is seen that these instances correspond to when there is a strong secondary maximum at $\beta = 1$ for the deep receiver. When the internal waves force a greater fraction of the total acoustic energy into the higher order, surface interacting modes, the $\beta = 1$ content in the observation increases regardless of receiver depth.

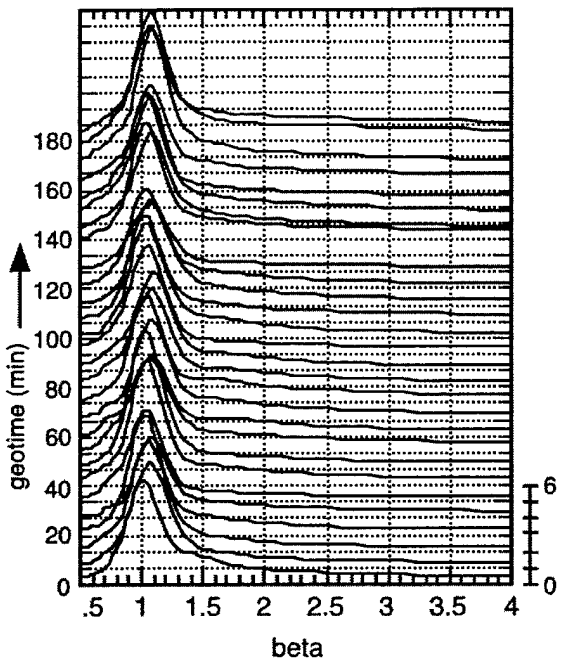

Figure 6. Effect of evolving background internal waves on intensity invariant. Same simulation parameters as in Fig. 5, except receiver depth changed to 10 m.

4.b. Bottom Attenuation

At all but the shortest of ranges in shallow water, interaction with the seabed cannot be neglected. A sandy bottom, as used in these simulations, will usually be acoustically faster than the water column. There is a finite loss associated with the bottom, often expressed in decibels-per-wavelength. A modal decomposition of the acoustic field for this situation shows that the modes penetrate into the seabed; as an example, see Fig. 2. In general, higher order modes penetrate further into the bottom than lower order modes. Consequently, the rate at which the modes attenuate as they propagate in range tends to increase with mode number. The bottom attenuation 0.04 dB/λ used in the simulations was based on the average value observed in the 1995 Shallow Water Acoustics in a Random Medium Experiment [26,27]. To test the sensitivity of the beta distribution to this parameter, the simulations were repeated using the same internal wave field but with increased bottom attenuation.

The simulation parameters in Figure 7 are the same as in Figure 5 except that the bottom loss has been increased to 0.1 dB/λ. Both the source and receiver are below the thermocline. As in the previous figure, the results are normalized by the energy in the corresponding range-independent case.

Even with the increased bottom attenuation, the peak in the distribution at $\beta = 1.5$ remains. The amplitude of the distribution at the peak, however, has been reduced. The increased attenuation disproportionately affects the higher order modes. The higher order modes provide the detailed, high spatial frequency features in the image. By diminishing these modes, the distribution becomes more diffuse. The effect of bottom loss is also evident in the secondary maximum at $\beta = 1$. While still occasionally present, the amplitude of the distribution at $\beta = 1$ is always clearly less than at $\beta = 1.5$. Again, this is because the higher order modes that contribute to the maximum at $\beta = 1$ have been attenuated.

The simulation was repeated with the bottom loss increased to 0.4 dB/λ. For this case (not shown), the distribution was diffuse with no distinct maxima at either $\beta = 1$ or $\beta = 1.5$. In such a

high loss environment, the concept of a waveguide invariant becomes problematic whether or not internal waves are present.

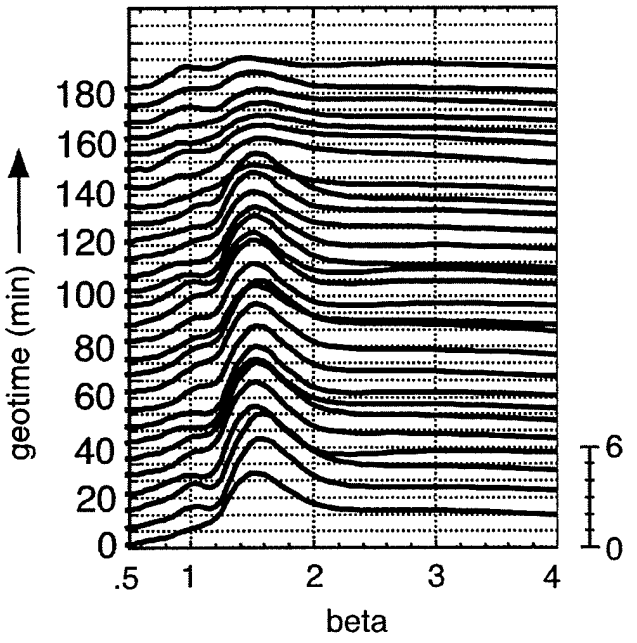

Figure 7. Effect of evolving background internal waves. Same as Fig. 5 except bottom loss increased to 0.1 dB/λ.

4.c. Range

From (3), increasing the range to the receiver should decrease the slope of the striations if beta is to remain invariant. Figure 8 shows a calculation for a data window extending from 20 to 21 km downrange, and from 400 to 420 Hz. Except for the increased range, the simulation parameters are the same as in Figure 5. Both source and receiver are below the thermocline at depth 50 m and the bottom attenuation is 0.04 dB/λ.

Comparing Figures 5 and 8, several observations can be made. The peak is generally sharper at the more distant range. Because the length of the receiving aperture is effectively a smaller fraction of the range to the source, there is less smoothing and the distribution becomes sharper. This is consistent with the formula derived in Rouseff and Spindel for the range-independent case [16]. The location of the peak, however, has shifted to a slightly higher value of beta. By going further in range, the higher order modes have been further attenuated. The lower order modes corresponding to higher values for beta have been less impacted. Finally, as one would expect, there is greater temporal variability. By increasing the range, the acoustic field encounters more internal waves and so acquires increased fluctuations.

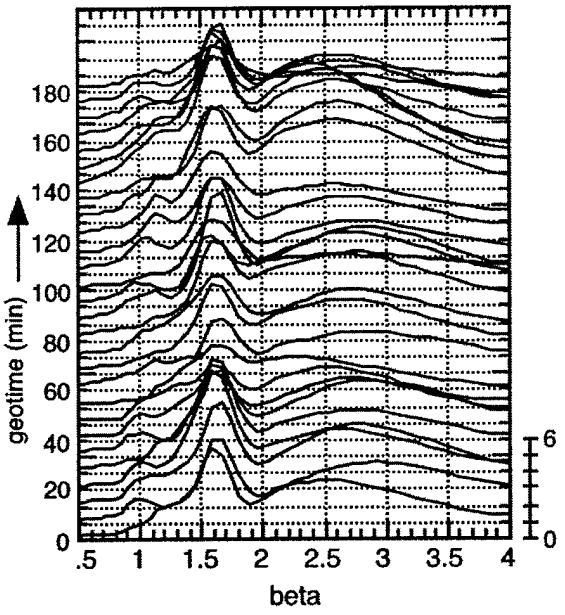

Figure 8. Effect of evolving background internal waves at increased range. Same simulation parameters as in Fig. 5 except data window extends from 20 to 21 km.

5. Effect of Discrete Internal Wave Packets

In addition to a background internal wave field, there is frequently another type of internal wave present in shallow water. Driven by tides and propagating from distinct bathymetric features, discrete packets of internal waves can be generated. Satellite images have shown that these waves can retain their coherence over multiple tidal cycles [28]. These solitary internal waves exhibit bore-like properties, hence the term "solibore" has been coined [29].

It remains an open research question as how to best model acoustic propagation through solibores. Both deterministic and stochastic approaches have been proposed [30]. The rudimentary model used in this paper is a hybrid. The solibore is modeled as an internal wave packet that in turn is the sum of several individual solitary waves. Each solitary wave depresses the background sound speed profile. The entire packet moves at constant velocity without changing shape; over the time scales of interest, dispersion is negligible. While the details of the internal wave packet—the amplitude of the individual solitary waves and the spacing between them—may be random, the direction and velocity of the packet is assumed known and deterministic. The information deemed deterministic could reasonably be gleaned from satellite images.

In the present study, the simple analytical model developed by Presig and Duda [31,32] is employed. Let d be the distance coordinate (range) relative to the leading edge of a solitary wave packet. The vertical depression $\zeta(d)$ within the packet is modeled as the sum of three solitary waves:

$$\zeta(d) = \sum_{i=1}^{3} a_i \mathrm{sech}^2[(d - d_i)/b_i], \tag{18}$$

where the numerical values used for a_i, b_i, and d_i are listed in Table I. Relative to the leading edge of the packet, the range-dependent sound speed profile (in m/s) in the water column $c(z,d)$ is modeled as being piecewise linear

$$c(z,d) = \begin{cases} 1522, & 0 < z < z_U + \zeta \\ 1522 + \Delta(z - (z_U + \eta)), & z_U + \zeta < z < z_L + \zeta \\ 1494, & z_L + \zeta < z < z_B \end{cases} \quad (19)$$

where the sound-speed gradient $\Delta = 28/(z_L - z_U)$, $z_U = 15$ m and $z_L = 30$ m. The water depth is the constant $z_B = 70$ m. The ocean sediment has constant sound speed 1580 m/s, density 1.85 g/cm^3, and attenuation 0.04 dB/λ. The model is identical to the one used by Preisig and Duda except the water depth and sediment parameters have been changed to be consistent with the simulations of the previous sections. The packet is assumed to propagate towards the acoustic source with constant velocity u. Consequently, at any time t the leading edge of the packet is at range $r = r_i - ut$, where r_i is the initial position. Consistent with observations in both the SWARM [27] and Coastal Mixing and Optics experiments [21,22], u=0.6 m/s is used.

i	a_i [m]	b_i [m]	d_i [m]
1	15	100	900
2	12	125	1400
3	10	150	2000

Table I. Parameters of soliton packet model.

While an obvious simplification, the model has two elements essential in the present application. First, as Preisig and Duda demonstrated, this model produces strong coupling between the acoustic modes. Second, the motion of the packet introduces temporal variability.

Figure 9 shows the internal wave model and its effect on the interference pattern. Figure 9(a) shows the vertical depression defined by (18). The leading edge of the packet and three subsequent depressions are indicated. As before, the intensity is measured over an aperture from 9 to 10 km in range and from 400 to 420 Hz in frequency. The source and receiver are below the thermocline at depth 50 m and the attenuation is 0.04 dB/λ. The initial position of wave packet is r_i=10 km. Figures 9(b)-(d) show the changing range-frequency plots of acoustic intensity as observed over the aperture while the packet moves. Superimposed on each plot is the $\beta = 1.5$ line. Figure 9(b) shows what is, in effect, the range-independent situation that occurs before the wave packet enters the range-frequency data window. Figure 9(c) shows the data window 40 minutes later. The internal wave packet has moved from right to left in the data window; the positions of the first two solitary wave depressions are as indicated. As one would expect, to the left of the first depression Figs. 9(b) and 9(c) are nearly identical. Figure 9(d) shows the data window just 10 minutes later. The new positions for the solitary wave depressions are as shown. The intensity pattern has changed noticeably in the wake of the internal waves. The results are indicative of the rapid changes in the acoustic intensity that can be caused by solitary waves. The solitary waves cause strong acoustic mode coupling. As this mode coupling structure moves, the acoustic interference pattern changes.

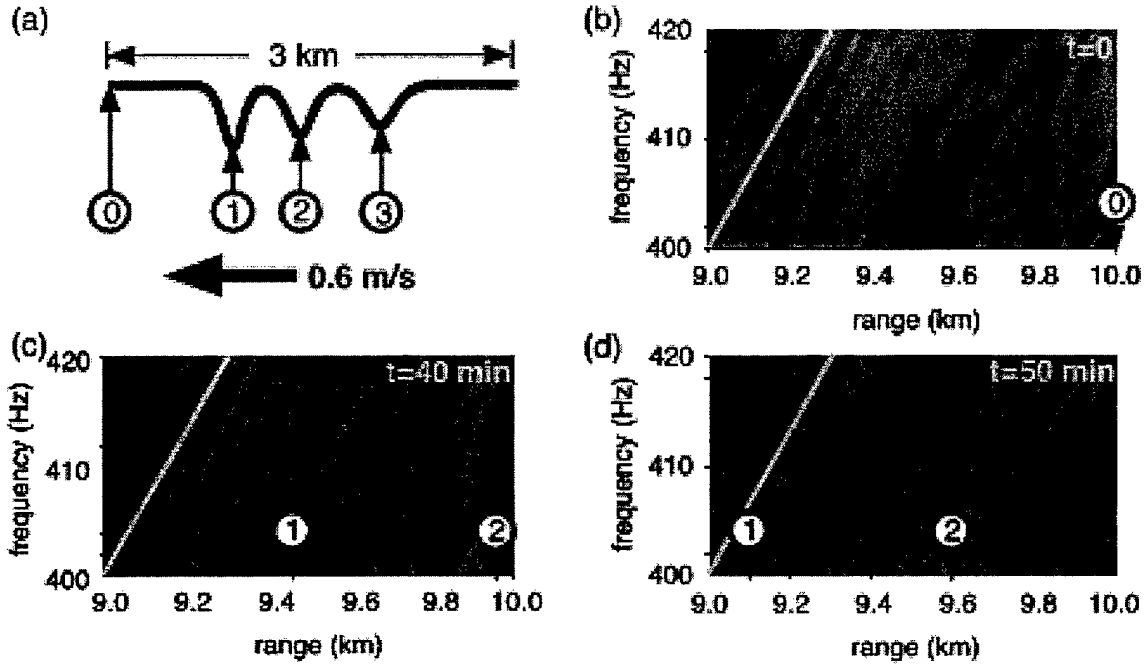

Figure 9. Evolution of intensity images caused by moving solitary wave packet. Solitary wave packet shown in (a). Point 0 denotes the leading edge with the subsequent sound speed depressions from Eq. (18) enumerated. Figs. (b)-(d) show intensity images at indicated times (in minutes) with leading edge and subsequent depressions positioned as indicated. Lines in (b)-(d) correspond to beta equal 1.5. In all cases, source and receiver are at depth 50 m. The same color scale with 16 dB dynamic range used in all plots.

In Figs. 9(c) and (d), the solitary waves are moving directly over the horizontal receiving array. In Fig. 10, the solitary waves have been allowed to continue moving towards the acoustic source. Shown is the beta content of the intensity images evolving over one-half hour, starting at t=100 minutes. For r_i=10 km and u=0.6 m/s, this corresponds to the packet moving just over 1 km, with the leading edge going from r=6400 m to r=5320 m. The time step between curves is one minute. With this sampling, there is considerable variability from curve to curve. Individual plots typically exhibit a broad distribution of values for β. Note that the maximum value for the individual plots is typically much less than observed in Fig. 5, a case that had similar simulation parameters but without the solitary waves. There is no obvious persistent maximum near β=1.5. Unless a more sophisticated processing scheme can be developed, solitary waves make it difficult to identify an invariant.

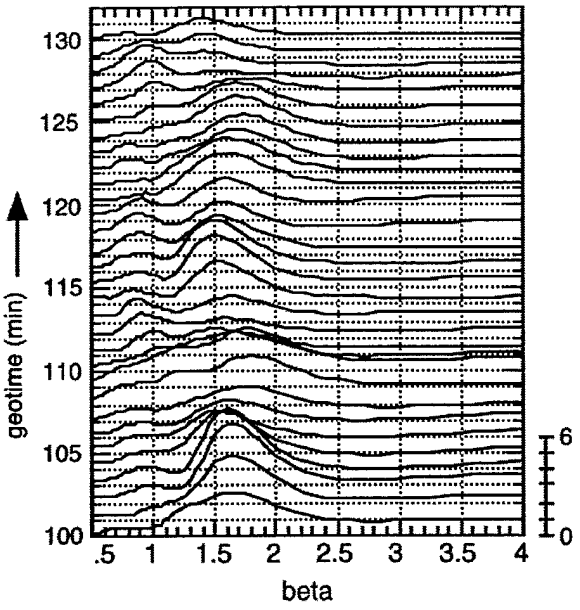

Figure 10. Effect of solitary internal waves on intensity invariant. Time step between curves is one minute.

6. Summary

Brekhovskikh and Lysanov [1] cautioned that there were limitations to the waveguide invariant defined by (1). If the frequency or range change, "the sound field will be determined by another group of modes...result[ing] in a change of β." In a similar fashion, the coupling of energy between acoustic modes can effectively change beta even if the frequency and range are fixed. The goal of the present work has been to study if the waveguide invariant can still be a practical tool at the level of the mode coupling introduced by shallow water internal waves.

Depending on the configuration, random background internal waves can cause an assortment of effects. If the source and receiver are appropriately placed relative to the thermocline, the internal waves can actually enhance the striations and sharpen the waveguide distribution. In other cases, the waveguide distribution can become bimodal making it appear as if there were two acoustic sources. In general, however, while the random background internal waves induce fluctuations in the invariant, they do not inherently destroy the concept. Packets of discrete solitary internal waves are more problematic. These waves introduce strong mode coupling and rapid variability in the acoustic interference pattern. For the simulation parameters considered, a definitive invariant could not be identified in the presence of solitary waves.

Acknowledgments

Steve Reynolds assisted in writing the section on background internal waves and performed the associated ocean simulations. This work was supported by the United States Office of Naval Research.

References

[1] Brekhovskikh L M and Lysanov Y P 1991 *Fundamentals of Ocean Acoustics,* 2nd ed. (New York: Springer-Verlag) pp. 140-145

[2] Chuprov S D 1982 Interference structure of a sound field in a layered ocean, in *Ocean Acoustics. Current State* ed L M Brekhovskikh and I B Andreevoi (Moscow: Nauka) pp. 71-91

[3] Burenkov S V 1989 Distinctive features of the interference structure of a sound field in a two-dimensionally inhomogeneous waveguide *Sov. Phys. Acoust.* **35** 465-467

[4] Malkina I G and Shevtsov V P 1989 Stability of the interference structure of the sound field in a shallow sea *Sov. Phys. Acoust.* **35** 506-509

[5] Goland V I 1991 Influence of the model of a random medium on the interference structure of a sound field in an acoustic waveguide *Sov. Phys. Acoust.* **37** 33-37

[6] Kuz'kin V M 1995 The effect of variability of ocean stratification on a sound field interference structure *Acoust. Phys.* **41** 300-301

[7] Kuperman W A, D'Spain G L, Song H C and Thode A M 1999 Application of the waveguide invariant approach *J. Acoust. Soc. Am.* **105** 983

[8] Hodgkiss W S, Song H C, Kuperman W A, Akal T, Ferla C and Jackson D R 1999 A long-range and variable focus phase-conjugation experiment in shallow water *J. Acoust. Soc. Am.* **105** 1597-1604

[9] D'Spain G L and Kuperman W A 1999 Application of waveguide invariants to analysis of spectrograms from shallow water environments that vary in range and azimuth *J. Acoust. Soc. Am.* **106** 2454-2468

[10] Petnikov V G and Kuz'kin V M 2002 Shallow water variability and its manifestation in interference pattern of sound field, to appear in *Ocean Acoustic Interference Phenomena and Signal Processing* ed W A Kuperman and G L D'Spain (AIP Press)

[11] Kuz'kin V M, Ogurtsov A V and Petnikov V G 1998 The effect of hydrodynaic variability on frequency shifts in the interference pattern of a sound field in a shallow sea *Acoust. Phys.* **44** 94-100

[12] Kuz'kin V M and Petnikov V G 1994 Frequency scale estimations of a sound field interference structure in a shallow sea *Acoust. Phys.* **40** 75-78

[13] Ishimaru A 1978 *Wave Propagation and Scattering in Random Media* (San Diego: Academic Press) p. 437

[14] Kak A C and Slaney M 1988 *Principles of Computerized Tomographic Imaging* (New York: IEEE Press) pp. 49-112

[15] Thode A M 2000 Source ranging with minimal environmental information using a virtual receiver and waveguide invariant theory *J. Acoust. Soc. Am.* **108** 1582-94

[16] Rouseff D and Spindel R C 2002 Modeling the waveguide invariant as a distribution, to appear in *Ocean Acoustic Interference Phenomena and Signal Processing* ed W A Kuperman and G L D'Spain (AIP Press)

[17] Munk W H 1981 Internal waves and small-scale processes, in *Evolution of Physical Oceanography* ed B A Warren and C Wunsch, (Cambridge, MA: MIT Press) pp. 264-291

[18] Henyey F S, Rouseff D, Grochocinski J M, Reynolds S A, Williams K L, and Ewart T E 1997 Effect of internal waves and turbulence on a horizontal aperture sonar *IEEE J. Oceanic Eng.* **22** 270-280

[19] Yan J, Zhang R, Zhou R S and Sha L 1999 Characteristics of the internal waves and their effects on the sound transmission in the midst of the Yellow Sea *Chinese J. of Acoustics* **18** 47-55

[20] Yang T C and Yoo K 1999 Internal wave spectrum in shallow water: measurement and comparison with the Garrett-Munk model *IEEE J. Oceanic Eng.* **24** 333-345

[21] Levine M and Boyd T, personal communication.

[22] Williams A J and Dickey T D, editors 2000 Special Issue on Coastal Mixing and Optics Experiment *J. Geophys. Res.*

[23] Gordon R L 1978 Internal wave climate near the coast of northwest Africa during JOINT-*I Deep Sea Res.* **23** 625-643

[24] Winters K B and E. D'Asaro E 1997 Direct simulation of internal wave energy *transfer J. Phys. Oceanog.* **27** 270-280

[25] Flatte' S M (ed), Dashen R, Munk W H, Watson K M and Zachariasen F 1979 *Sound Transmission through a Fluctuating Ocean* (Cambridge: Cambridge University Press) p. 59

[26] Apel J R, et al 1997 An overview of the 1995 SWARM shallow-water internal wave acoustic scattering experiment *IEEE J. Oceanic Eng.* **22** 465-500

[27] Headrick R H, et al. 2000 Modeling mode arrivals in the 1995 SWARM experiment acoustic transmissions *J. Acoust. Soc. Am.* **107** 221-236

[28] Liu A K 1988 Analysis of nonlinear internal waves in the New York Bight *J. Geophys. Res.* **93** 12317-12329

[29] Henyey F S and Hoering A 1997 Energetics of borelike internal waves *J. Geophys. Res.* **102** 3323-3330

[30] Lynch J F 1997 Report of the Office of Naval Research Shallow-Water Acoustic Workshop 1-3 October 1996, *Woods Hole Oceanographic Institution Technical Report WHOI-97-12*

[31] Preisig J C and Duda T F 1997 Coupled acoustic mode propagation through continental-shelf internal solitary waves *IEEE J. Oceanic Eng.* **22** 256-269

[32] Duda T F and Preisig J C 1999 A modeling study of acoustic propagation through moving shallow-water solitary wave packets *IEEE J. Oceanic Eng.* **24** 16-32